CMS Technical Summary Report #94-8

OSCILLATIONS IN PISTON-DRIVEN SHEAR FLOW OF A NON-NEWTONIAN FLUID

David S. Malkus, John A. Nohel
and Bradley J. Plohr

UNIVERSITY OF WISCONSIN

CENTER FOR THE MATHEMATICAL SCIENCES

Center for the Mathematical Sciences
University of Wisconsin—Madison
1308 W. Dayton Street
Madison, Wisconsin 53715-1149

February 1994

(Received February 8, 1994)

Approved for public release
Distribution unlimited

Sponsored by

U.S. Army Research Office
P. O. Box 12211
Research Triangle Park
North Carolina 27709

National Science Foundation
1800 G. Street
Washington, DC 20550

U. S. Department of Energy
Washington, DC 20545

UNIVERSITY OF WISCONSIN-MADISON
CENTER FOR THE MATHEMATICAL SCIENCES

OSCILLATIONS IN PISTON-DRIVEN SHEAR FLOW OF A NON-NEWTONIAN FLUID

David S. Malkus
John A. Nohel
Bradley J. Plohr

CMS Technical Summary Report #94-8

February 1994

AMS (MOS) Subject Classications: 34C35, 34K35, 65N30,76A05, 76A10

Key Words and Phrases: Shear flow, piston-driven, non-Newtonian, non-monotone, oscillations, spurt, feedback control, quadratic systems, Hopf bifurcation, periodic orbits.

This work was supported in part by: the National Science Foundation under Grant DMS-9216153; the National Science Foundations under Grant DMS-9201581; the National Science Foundation under Grant INT-9216357; the U.S. Army Research Office under Grant DAAL03-92-G-0185; the U.S. Army Research Office under Grant DAAL03-91-C-0027 to the Mathematical Sciences Institute of Cornell University, through subcontract to Stony Brook; and the Applied Mathematics Subprogram of the U.S. Department of Energy under Grant DE-FG02-90ER25084.

OSCILLATIONS IN PISTON-DRIVEN SHEAR FLOW OF A NON-NEWTONIAN FLUID

DAVID S. MALKUS
JOHN A. NOHEL
BRADLEY J. PLOHR

ABSTRACT. In recent experiments on piston-driven shear flow of a highly elastic and very viscous non-Newtonian fluid, Lim and Schowalter observed nearly periodic oscillations in the particle velocity at the channel wall for particular values of the constant volumetric flow rate. Such periodicity has been characterized as a "stick/slip" phenomenon caused by the failure of the fluid to adhere to the wall. We suggest an alternative explanation for these oscillations using a dynamic mathematical model based on the Johnson-Segalman-Oldroyd constitutive relation, the key feature of which is a non-monotonic relationship between steady shear stress and strain rate. The resulting three-dimensional equations of motion and stress are reduced to one space dimension, consistent with experimental results. In the inertialess approximation, the equations governing the flow can be viewed as a continuous family of quadratic ordinary differential equations coupled by the non-local constraint that fixes the volumetric flow rate. Varying the flow rate, the numerical simulation of solutions to this system exhibits transitions to and from a regime with persistent oscillations that compare favorably with the Lim-Schowalter observations. When the time-asymptotic behavior is cyclic, large shear strain rates are observed in a thin but macroscopic layer near the wall. The transitions are explained using spectral analysis of the linear (infinite dimensional) operator resulting from linearization of the quadratic system about a discontinuous steady state with a jump discontinuity in the stress components. The persistent oscillations arise as a Hopf bifurcation to periodic orbits as the volumetric flow rate is increased beyond a critical value.

1. INTRODUCTION

In their recent experiments on piston-driven flow at a fixed volumetric flow rate of a highly elastic and very viscous non-Newtonian fluid, F. Lim and W. Schowalter [4, 5] observed persistent, nearly periodic oscillations in the particle velocity near the channel wall. They characterized the periodicity as a stick/slip phenomenon; oscillations are thought to reflect periodic detachment and reattachment of the fluid, while the regular temporal variation of normal stresses leads to spatially periodic distortion of the extrudate [1].

1980 *Mathematics Subject Classification* (1985 *Revision*). 34C35, 34K35, 65N30, 76A05, 76A10

Key words and phrases. Shear flow, piston-driven, non-Newtonian, non-monotone, oscillations, spurt, feedback control, quadratic systems, Hopf bifurcation, periodic orbits.

This work was supported in part by: the National Science Foundation under Grant DMS-9216153; the National Science Foundation under Grant DMS-9201581; the National Science Foundation under Grant INT-9216357; the U. S. Army Research Office under Grant DAAL03-92-G-0185; the U. S. Army Research Office under Grant DAAL03-91-C-0027 to the Mathematical Sciences Institute of Cornell University, through subcontract to Stony Brook; and the Applied Mathematics Subprogram of the U. S. Department of Energy under Grant DE-FG02-90ER25084.

In this paper, our focus is on mathematical modeling of the Lim-Schowalter experiment, in which the volumetric flow rate is prescribed by driving the fluid with a piston moving at fixed speed. Experimental data suggest that far away from the piston, the flow is essentially one-dimensional. Highly elastic and very viscous non-Newtonian materials are modeled mathematically as incompressible viscoelastic fluids with fading memory and, for the present, under isothermal conditions. The basis for our explanation of persistent oscillations in piston-driven flow is the differential Johnson-Segalman-Oldroyd constitutive law, which is consistent with experimental shear data; it exhibits a non-monotonic relation between steady shear stress and strain rate. This constitutive model has already been used successfully by us in Refs. [6, 7, 12] to provide an alternative explanation of "spurt" and related phenomena, originally observed in experiments by G. Vinogradov *et al.* [14] in pressure-gradient driven flows. (While the Johnson-Segalman-Oldroyd constitutive model performs well in reproducing particular shear flows of highly elastic and viscous non-Newtonian fluids, we neither claim nor expect that it will perform equally well in other flows (*e.g.*, extensional flow).)

Piston-driven flow at a fixed volumetric flow rate is modeled as an instantaneous, globally well-posed feedback-control problem in one space dimension, the control being the prescribed volumetric flow rate and the feedback being the pressure gradient. A deeper analytical understanding of the governing equations is possible because the system contains a small parameter, the ratio of Reynolds number to Deborah number. In the inertialess approximation, obtained by setting this parameter to zero, the equations governing the flow can be viewed as a continuous family of quadratic ordinary differential equations coupled by the non-local constraint that fixes the volumetric flow rate; all solutions of this system are bounded, even for large, discontinuous initial data. Numerical simulations demonstrate that beyond a critical flow rate, the time-asymptotic behavior is cyclic. Large shear strain rates are observed in a thin, but macroscopic, layer near the wall; such a layer also appears in pressure-driven spurt flow.

Further analysis of the inertialess system links the observed oscillations to the occurrence of a Hopf bifurcation that spawns a periodic orbit beyond a critical flow rate. To understand this behavior, we observe that the dynamic equations admit discontinuous steady states when the volumetric flow rate is fixed (corresponding to the wall stress between the steady local shear stress maximum and minimum), and we linearize the system around a discontinuous steady state with a single jump. Parametrizing such discontinuous steady states by wall stress and flow rate, there are regions in parameter space in which the eigenvalues of the discrete spectrum of the linearized operator change from having negative real parts to having positive real parts, and there is a separating curve along which the real part of the eigenvalue vanishes. This information is the basis for showing in Ref. [10] that a Hopf bifurcation to a periodic orbit occurs when the flow rate is raised beyond a critical value. However, proving that the resulting periodic orbit is stable (*i.e.*, that the bifurcation is supercritical) remains a challenging open problem.

The outline of this paper is as follows. In Sec. 2, we summarize the development the mathematical model for unsteady, isothermal, piston-driven planar channel flow of a highly elastic and viscous non-Newtonian fluid, based on balance laws and the Johnson-Segalman–Oldroyd differential constitutive law, with a single relaxation time, in three dimensions. The

inertialess approximation for such a flow takes the form of a one-parameter quadratic system of first-order functional differential equations in which the fixed volumetric flow rate is imposed as the control and the pressure gradient is the feedback. In Sec. 3, a two-parameter family of discontinuous steady state flows is determined. The two parameters can be chosen to be the volumetric flow rate and the position of the stress discontinuity. In Sec. 4, we use a numerical algorithm for the inertialess system to simulate piston-driven flows. We consider the sudden start-up problem, in which the volumetric flow rate is instantaneously raised from zero and then held fixed. Upon varying the fixed volumetric flow rate, the numerical simulation of solutions exhibits transitions to and from a regime with persistent oscillations; this phenomenon compares favorably with the Lim-Schowalter observations. In Sec. 5, spectral properties of the inertialess system linearized about particular discontinuous steady states are determined. The infinite dimensional linearized operator is bounded, and we determine criteria for its essential and discrete spectra analytically. We use a numerical method to compute the discrete spectrum of the linearized operator from the analytical criterion. The discrete spectrum consists of a pair of simple, complex conjugate eigenvalues, and the sign of the real parts of these eigenvalues changes from negative to positive along a curve within the parameter plane for the discontinuous steady states. In Sec. 6, we relate the results on the discrete spectrum obtained in Sec. 5 to results of numerical simulations in Sec. 4, and we explain the experimentally observed persistent oscillations as a Hopf bifurcation occurring when the control parameter is increased beyond a critical value. Finally, in Sec. 7, we use the results of Secs. 5 and 6 to offer an alternative explanation of the mechanism underlying the Lim-Schowalter experiment.

2. Piston-Driven Shear Flow

To model the experiments of Lim and Schowalter, we consider the planar Poiseuille flow a channel of a highly elastic and very viscous incompressible non-Newtonian fluid under isothermal conditions, satisfying the Johnson-Segalman–Oldroyd constitutive relations for the evolution of the extra stress tensor. We summarize the derivation of the system of partial differential equations that governs such a one-dimensional shear flow, starting from balance laws and constitutive equations in three dimensions; for more details, see Refs. [6, 7].

The channel is aligned along the y-axis and extends between $x = -h/2$ and $x = h/2$. The flow is assumed to be symmetric about the centerline $x = 0$ of the channel, and we restrict attention to the interval $x \in [-h/2, 0]$. Since the fluid undergoes simple shearing, the velocity and stress variables are independent of y. In particular, the velocity field is $\mathbf{v} = (0, v(x,t))$, so that the flow is incompressible and the conservation of mass equation is automatically satisfied.

The total shear stress on the fluid is the sum of three contributions, an isotropic pressure, a Newtonian stress, and an extra stress π. The conservation of momentum in the x-direction implies that the pressure takes the form $p = p_0(x,t) - f(t)\,y$, with f being the pressure gradient. We adopt the Johnson-Segalman–Oldroyd differential constitutive law with a single relaxation time [13, 2] to determine the extra stress. In shear flow, the extra stress is expressible in terms of two variables, the shear stress $\sigma(x,t) := \pi^{xy}$ and the principal normal

stress difference $Z(x,t) := -\frac{1}{2}(1-a^2)(\pi^{yy}-\pi^{xx})$; here $a \in (-1,1)$ is the slip parameter of the fluid. The fluid variables v, σ, and Z are governed by the y-momentum equation and constitutive differential equations. We introduce two dimensionless parameters that characterize the flow: α, the ratio of Reynolds number to Deborah number; and ε, the ratio of Newtonian viscosity to shear viscosity. After suitable scaling, the governing equations become

$$\begin{aligned} \alpha v_t - \sigma_x &= \varepsilon v_{xx} + f \ , \\ \sigma_t - (Z+1)v_x &= -\sigma \ , \\ Z_t + \sigma v_x &= -Z \ . \end{aligned} \tag{JSO}$$

on the interval $[-1/2, 0]$. The boundary conditions are

$$v(-1/2, t) = 0 \quad \text{and} \quad v_x(0,t) = 0 \ . \tag{BC}$$

At $t = 0$, we impose the initial conditions

$$v(x,0) = v_0(x) \ , \quad \sigma(x,0) = \sigma_0(x) \ , \quad \text{and} \quad Z(x,0) = Z_0(x) \ . \tag{IC}$$

For consistency of (IC) with (BC), we assume that $v_0(-1/2) = 0$ and $v_0'(0) = 0$; to maintain continuity at $x = 0$, we require that $\sigma_0(0) = 0$. This condition, together with the boundary condition $v_x(0,t) = 0$ and the second equation of system (JSO), implies that $\sigma(0,t) = 0$ for all t. Thus symmetry about the centerline in maintained.

In the case of highly elastic polymer systems, α is very small, 7 to 10 orders of magnitude smaller than ε, which itself is of the order of 10^{-3}. Throughout this paper, therefore, we make the inertialess approximation $\alpha = 0$. This approximation has been used successfully in Refs. [7, 12] to study pressure-driven flow in which the pressure gradient f is prescribed. If $\alpha = 0$, the momentum equation in system (JSO), combined with the boundary conditions (BC) and $\sigma(0,t) = 0$, implies that

$$v_x = \frac{T - \sigma}{\varepsilon} \ , \tag{2.1}$$

where

$$T(x,t) := -f(t)x \tag{2.2}$$

coincides with the total shear stress $\sigma + \varepsilon v_x$. Using Eq. (2.1), v_x can be eliminated from system (JSO).

In piston-driven flow, the volumetric flow rate Q is prescribed, Q being given by

$$Q(t) := 2\int_{-1/2}^{0} v(x,t)\,dx = -2\int_{-1/2}^{0} x v_x(x,t)\,dx \ ; \tag{2.3}$$

here an integration by parts was carried out in the second step. However, the pressure gradient f is not known; instead, f adjusts to maintain the desired flow rate Q. We can express f, or equivalently T, in terms of the given flow rate Q as follows. Substituting for v_x in Eq. (2.3) using Eq. (2.1) leads to the feedback equation

$$T(x,t) = -12\varepsilon Q(t)x + 24x\int_{-1/2}^{0} y\sigma(y,t)\,dy \ . \tag{FB}$$

where we think of the prescribed Q as the control and f (or equivalently T) as the feedback. This equation is written more simply as $T = T_0 + P\sigma$, where $T_0(x,t) := -12\varepsilon Q(t)x$ and where the operator P, defined by

$$[P\sigma](x,t) := 24x \int_{-1/2}^{0} y\sigma(y,t)\,dy \tag{2.4}$$

is a projection, in the sense that $P^2\sigma := P[P\sigma] = P\sigma$.

Thus the system governing inertialess piston-driven flow is the quadratic system of functional differential equations

$$\begin{aligned} \sigma_t &= (Z+1)\left(\frac{T-\sigma}{\varepsilon}\right) - \sigma\,, \\ Z_t &= -\sigma\left(\frac{T-\sigma}{\varepsilon}\right) - Z\,, \\ T &= T_0 + P\sigma\,, \end{aligned} \tag{QFDE}$$

together with prescribed the initial conditions (IC) for $\sigma(x,0), Z(x.0)$.

Throughout the rest of this paper, we will assume that the prescribed flow rate $Q(t) = \overline{Q}$ is a positive constant. It is shown in Ref. [9] that the initial value problem for $(QFDE)$ is globally well posed for all time and for initial data σ_0, Z_0 that are either smooth or rough (in the sense of being only bounded and measurable) and of arbitrary size; moreover, the stress components σ, Z remain bounded. (We remark that the global well-posedness of the full governing system for piston-driven flow with $\alpha > 0$ is also discussed in Ref. [9].) Beyond technical considerations that need not concern us here, the key to proving global existence and boundedness of solutions and understanding the dynamics is that solutions of system $(QFDE)$ satisfy the Lyapunov-type identity

$$\frac{d}{dt}\left\{\sigma^2 + (Z+1)^2\right\} = -2\left[\sigma^2 + (Z+\tfrac{1}{2})^2 - \tfrac{1}{4}\right]\,. \tag{L}$$

Observe that Eq. (L) is independent of α, ε, and T. It follows easily from Eq. (L) that $\sigma(\cdot,t)$ and $Z(\cdot,t)$ remain bounded for as long as the solution σ, Z of system $(QFDE)$ exists. This fact, together with standard results, implies that every locally defined solution can be continued forward (uniquely) for all time; moreover, the solution remains bounded, the bound depending only on the size of the initial data. However, although solutions to system $(QFDE)$ exist globally and remain bounded, it is difficult to determine their asymptotic behavior of solutions as $t \to \infty$. Indeed, the extensive literature on quadratic differential and functional differential equations does include any results on the global qualitative structure of solutions of $(QFDE)$. The rest of this paper is devoted to understanding some of the interesting dynamics of the quadratic system $(QFDE)$ by a combination of analytical and numerical methods, and this leads to an explanation of the experimental observations of Lim and Schowalter.

3. Steady Flows.

Our goal is to study the linearized stability and instability of steady state solutions of system $(QFDE)$. It will be clear that steady states of (JSO) and of $(QFDE)$ coincide.

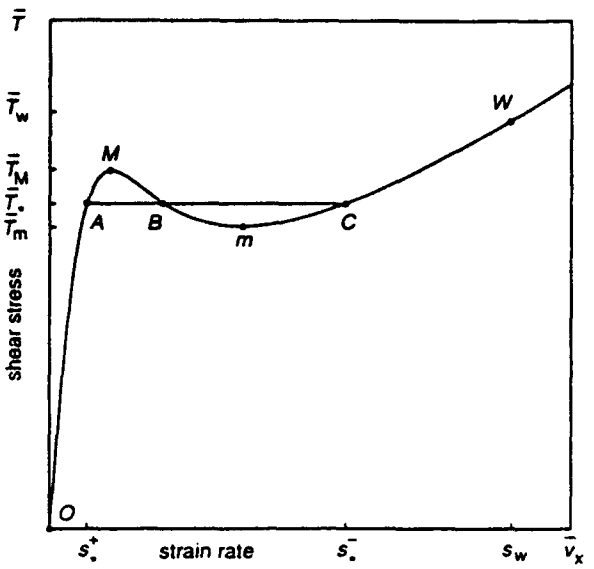

Fig. 1: The steady shear stress $\overline{T} = w(\overline{v}_x)$ plotted vs. shear strain rate $\overline{v}_x$.

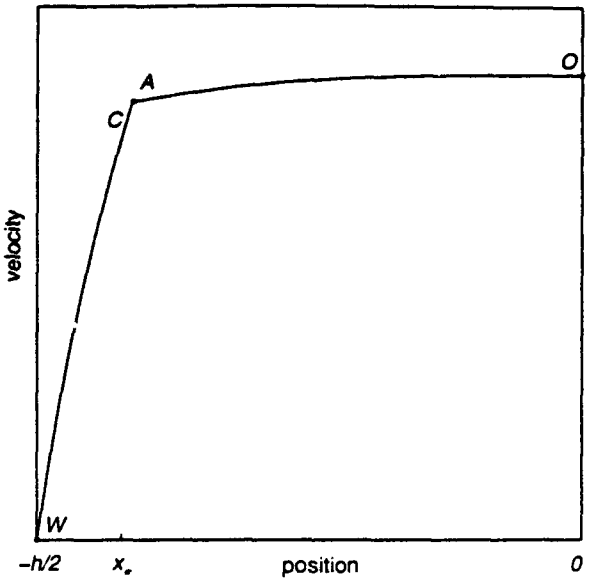

Fig. 2: The velocity profile in steady flow for the path $OACW$ shown in Fig. 1.

We shall indicate a steady state solution using an overbar. Taking $Q(t) := \overline{Q} > 0$ to be a constant and setting $\sigma_t = 0$ and $Z_t = 0$ in $(QFDE)$ shows that system $(QFDE)$ admits steady states $\overline{\sigma}, \overline{Z}$ satisfying the following requirements:

$$\overline{\sigma} = \frac{\overline{v}_x}{1+\overline{v}_x^2}\,, \qquad \overline{Z} = -\frac{\overline{v}_x^2}{1+\overline{v}_x^2}\,, \tag{3.1}$$

$$\overline{T} = \frac{\overline{v}_x}{1+\overline{v}_x^2} + \varepsilon \overline{v}_x\,, \qquad \overline{T} = \overline{T}_0 + P\overline{\sigma}\,, \tag{3.2}$$

where we define $\overline{T}_0(x) := -12\varepsilon \overline{Q} x$.

The steady strain rate $\overline{v}_x$ is determined by solving the steady stress/strain-rate relation

$$w(\overline{v}_x) = \overline{T}\,, \tag{3.3}$$

where the function w is defined by

$$w(s) := \frac{s}{1+s^2} + \varepsilon s\,. \tag{3.4}$$

When $\varepsilon < 1/8$, the function w is not monotone, as shown in Fig. 1. This leads to the occurrence of piecewise smooth steady state solutions with simple jump discontinuities in $\overline{v}_x$, implying a kink in the steady velocity $\overline{v}$; such a solution is indicated in Figs. 1 and 2. Formulae (3.1) imply that the steady stresses $\overline{\sigma}$ and $\overline{Z}$ are piecewise smooth functions having jump discontinuities whenever the strain rate $\overline{v}_x$ does.

While there are steady solutions with an arbitrary number of discontinuities, we focus on those with a single discontinuity. There is a two-parameter family of such solutions. It proves convenient to take as parameters the total stress $\overline{T}_* := \overline{T}(x_*)$ at the kink and the

thickness $\delta := x_* + 1/2$ of the layer of high strain rate. The region of allowable values for these parameters is rectangular: $\overline{T}_*$ lies between $\overline{T}_m$ and $\overline{T}_M$, the stresses at the minimum and maximum of w; and δ lies in the interval $[0, 1/2)$.

For each choice of $(\overline{T}_*, \delta)$, the strain rate $\overline{v}_x$ is determined by solving

$$w(\overline{v}_x(x)) = \overline{T}_* \frac{x}{x_*} \tag{3.5}$$

for each $x \in [-1/2, 0]$; here $x_* := -1/2+\delta$, and when there are multiple solutions of Eq. (3.5), $\overline{v}_x(x)$ is chosen on the high or low strain-rate branch of w according as $x < x_*$ or $x > x_*$. The function $\overline{v}_x$ determines $\overline{\sigma}$ and $\overline{Z}$ through Eqs. (3.1), and the flow-rate $\overline{Q}$ for the solution is calculated through Eq. (2.3).

A more convenient formula for $\overline{Q}$ can be obtained using a change of variables introduced by Yao [15]: in Eq. (2.3), change variables from x to $s := \overline{v}_x(x)$ using the relation $-\overline{f}x = w(s)$ to obtain

$$\overline{Q} = \frac{2}{\overline{f}^2} \int_{\mathcal{U}} s\, w(s) w'(s)\, ds \ , \tag{3.6}$$

where in the present application

$$\overline{f} = -\frac{\overline{T}_*}{x_*} = \frac{2\overline{T}_*}{1 - 2\delta} \ . \tag{3.7}$$

Here, the interval of integration is $\mathcal{U} := [0, s_*^+] \cup [s_*^-, s_w]$, where $s_*^\pm := \lim_{x \to x_*^\pm} \overline{v}_x(x)$ (the low and high strain-rate solutions of $w(s_*) = \overline{T}_*$) and $s_w := \overline{v}_x(-\frac{1}{2})$ (the high strain-rate solution of $w(s_w) = \overline{T}_w$), as in Fig. 1. The integral in Eq. (3.6) can be evaluated explicitly [15]:

$$\int_0^s t\, w(t) w'(t)\, dt = -\left(\tfrac{1}{4} - \varepsilon\right) \tan^{-1} s + \left(\tfrac{3}{4} - \varepsilon\right) \frac{s}{1 + s^2} - \tfrac{1}{2} \frac{s}{(1 + s^2)^2} + \tfrac{1}{3} \varepsilon^2 s^2 \ . \tag{3.8}$$

To make contact with experiment, however, it is preferable to use parameters different from $\overline{T}_*$ and δ, namely the total stress $\overline{T}_w := \overline{T}_*/(1 - 2\delta)$ at the channel wall and the flow rate $\overline{Q}$. (See Fig. 4a below.) The lines $\overline{T}_* = \overline{T}_m$, $\overline{T}_* = \overline{T}_M$, and $\delta = 0$, which bound the allowable region in the $(\overline{T}_*, \delta)$-plane, correspond respectively to the three curves labeled "bottom-jumping," "top-jumping," and "classical flow" in the $(\overline{T}_w, \overline{Q})$-plane.

4. Numerical Simulation of Piston-Driven Flows.

In order to motivate the analysis presented in subsequent sections, we first present results of numerically simulating the Lim-Schowalter experiment using system $(QFDE)$. The numerical algorithm (which was derived in Ref. [9]) is as follows. We predict v_x at time level $n + 1$ using the formula

$$(v_x)_{n+1} = \frac{T_n^k - \sigma_n^k}{\varepsilon} \tag{4.1}$$

for the k^{th} element in the mesh; here k runs from 1 to the number of elements, N, and σ_n^k is the value of the shear stress in the k^{th} element at time level n. For the given flow rate $\overline{Q}$, the stress T_n^k is computed by evaluating $P\sigma$ in system $(QFDE)$ using the midpoint rule:

$$T_n^k = \frac{(x_k + x_{k+1})}{2}\left(-12\varepsilon\overline{Q} + 24\sum_{i=1}^{N-1}\sigma_n^i\,(x_{i+1} - x_i)\,(x_i + x_{i+1})/2\right) . \tag{4.2}$$

We then difference and advance the stresses σ and Z, using the latest available value of $(v_x)_{n+1}$, by the following "corrector" scheme:

$$\begin{cases} \sigma_{n+1} = (1 - \Delta t)\sigma_n + \Delta t(Z_n + 1)(v_x)_{n+1} , \\ Z_{n+1} = (1 - \Delta t)Z_n - \Delta t\sigma_{n+1}(v_x)_{n+1} . \end{cases} \tag{4.3}$$

The basic simulation that we perform using the above algorithm idealizes the instantaneous start-up of a flow. In other words, the test apparatus is filled with fluid at rest, and then the flow rate is suddenly increased from zero to the prescribed value $\overline{Q}$. Therefore the initial conditions are $v_0(x) = \sigma_0(x) = Z_0(x) = 0$. To compare our results with the experimental results, we compute the pressure gradient f for each given flow rate $\overline{Q}$. In the simulations of $(QFDE)$, we observe four distinct flow regimes, corresponding to different values of the prescribed flow rate $\overline{Q}$: the classical, spurt I, oscillatory, and spurt II regimes. Typical plots of $f(t)$ vs. t in the four regimes are shown in Figs. 3a–d.

In the classical regime, continuous steady solutions are achieved. Steady solutions are also achieved in the spurt I and II regimes; they are, however, discontinuous and have the appearance of the spurt solutions achieved in pressure-gradient driven flows [6, 7]. As $\overline{Q}$ is increased and the transition to the oscillatory regime is approached, the time required for the flow to settle to a steady state increases, and the settling is accompanied by damped oscillations in $f(t)$ and in the velocity near the wall. Finally, at a critical value of $\overline{Q}$, the oscillations appear to become undamped and fail to settle down; this is the oscillatory regime. If $\overline{Q}$ is increased further, a second transition is observed, and steady, spurt-like solutions are again achieved; this is the spurt II regime. (For technical reasons, Fig. 3d terminates before the oscillations have died away to graphical accuracy; however, the simulation has been carried out for much longer time, and there is no doubt that the oscillations die out.)

We wish to stress that because we rely on numerical simulation, and because it is difficult to accurately distinguish slightly damped systems from undamped systems numerically, the existence of a true oscillatory regime for the full system $(QFDE)$ can only be conjectured at this point.

We studied transitions between these regimes in detail, as a function of the imposed volumetric flow rate $\overline{Q}$, for the polyisoprene sample PI-7 of Ref. [14] (*i.e.*, $\varepsilon = 0.001417$). As $\overline{Q}$ is increased from zero, the transition from the classical regime to the spurt I regime occurs at approximately $\overline{Q} = 0.1$. The transition between the steady spurt I regime and the oscillatory regime occurs at a critical $\overline{Q}$ of about 0.3, whereas the transition from the oscillatory regime back to the steady spurt II regime occurs at a critical $\overline{Q}$ of about 1.4. We emphasize that Lim [4] also observed four separate flow regimes in his experiments, the third of which is oscillatory and the fourth of which is a relatively steady regime at high shear rate (inferred from $\overline{Q}$). Thus our numerical simulation of $(QFDE)$ conforms qualitatively with experimental results.

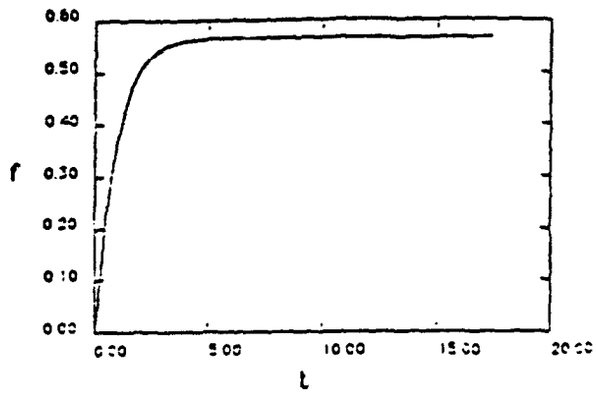

Fig. 3a: $f(t)$ *vs.* t in the classical regime of system $(QFDE)$.

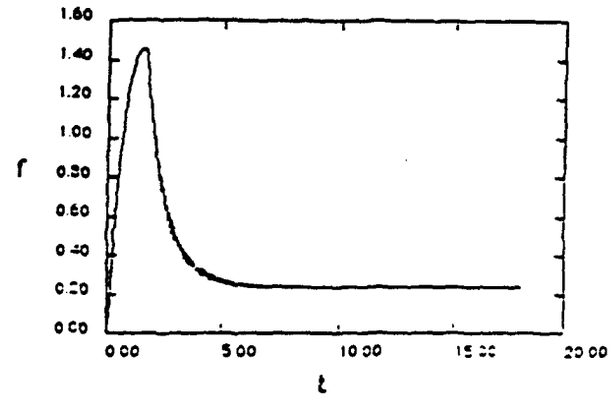

Fig. 3b: $f(t)$ *vs.* t in the spurt I regime of system $(QFDE)$.

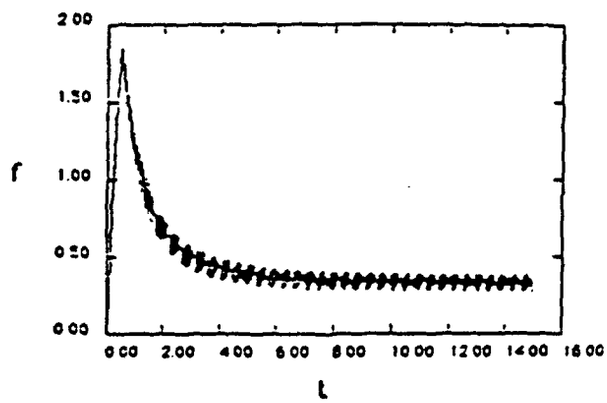

Fig. 3c: $f(t)$ *vs.* t in the oscillatory regime of system $(QFDE)$.

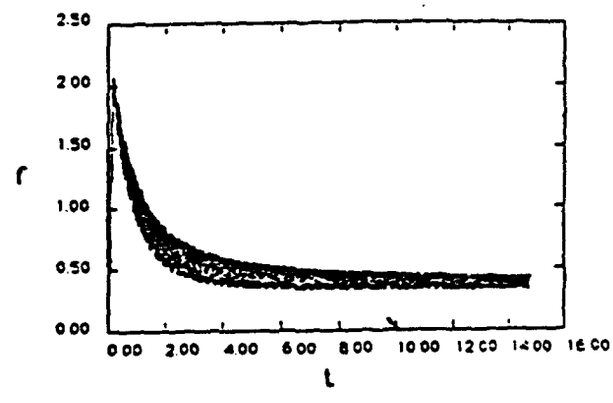

Fig. 3d: $f(t)$ *vs.* t in the spurt II regime of system $(QFDE)$.

5. Linearized Stability Analysis.

We consider a solution of system $(QFDE)$ that is a small perturbation of a piecewise smooth steady state $(\overline{\sigma}, \overline{Z})$; for simplicity, we assume that this steady state has a single jump discontinuity at x_*, at which point $\overline{T}(x_*) = \overline{T}_*$. We write $\sigma = \overline{\sigma} + \hat{\sigma}$ and $Z = \overline{Z} + \hat{Z}$. The linearized equations for $\hat{\sigma}$ and $\hat{Z}$ are

$$\begin{pmatrix} \hat{\sigma}_t \\ \hat{Z}_t \end{pmatrix} = L \begin{pmatrix} \hat{\sigma} \\ \hat{Z} \end{pmatrix} := J(\overline{\sigma}, \overline{Z}, \overline{T}) \begin{pmatrix} \hat{\sigma} \\ \hat{Z} \end{pmatrix} + \begin{pmatrix} (\overline{Z}+1)/\varepsilon \\ -\overline{\sigma}/\varepsilon \end{pmatrix} P\hat{\sigma} \,, \tag{5.1}$$

where

$$J(\overline{\sigma}, \overline{Z}, \overline{T}) := \begin{pmatrix} -1-(\overline{Z}+1)/\varepsilon & (\overline{T}-\overline{\sigma})/\varepsilon \\ (2\overline{\sigma}-\overline{T})/\varepsilon & -1 \end{pmatrix} . \tag{5.2}$$

The operator L is a bounded linear operator acting on the Hilbert space of pairs of functions $(\hat{\sigma}, \hat{Z}) \in \mathcal{X} := PS_{x_*} \times PS_{x_*}$, where $PS_{x_*} := H^1(-1/2, x_*) \times H^1(x_*, 0)$ is the space of piecewise smooth (*i.e.*, H^1) functions on the interval $[-1/2, 0]$ with a single jump discontinuity at x_*. The linearized stability of the steady state is determined by the spectral properties of L which we now summarize; the results stated below are proved in Ref. [10].

Since the linear operator L is bounded on $\mathcal{X}$, L is the generator of an analytic semigroup, and the time-asymptotic behavior of solutions of the linear system (5.1) is determined by the discrete spectrum of L. To find it, we also need to determine the essential spectrum of L. The first result states that the essential spectrum of L coincides with the set of eigenvalues of the Jacobian matrix J for every $x \in [-1/2, 0]$.

Proposition 5.1: *The essential spectrum of L is*

$$\sigma_{\text{ess}}(L) = \bigcup_{x \in [-1/2, 0]} \left\{ \lambda \in C \mid \lambda \text{ is an eigenvalue of } J(\overline{\sigma}(x), \overline{Z}(x), \overline{T}(x)) \right\} . \tag{5.3}$$

Furthermore, if $\overline{T}_* \neq \overline{T}_m$ and $\overline{T}_* \neq \overline{T}_M$ (i.e., the steady solution is neither bottom nor top jumping), then there exists an $\eta > 0$ such that $Re\,\lambda \leq -\eta$ for all $\lambda \in \sigma_{\text{ess}}(L)$.

The Jacobian matrix J is precisely the matrix analyzed in Ref. [7]. According to Prop. 3.2 of Ref. [7], the eigenvalues of $J(\overline{\sigma}(x), \overline{Z}(x), \overline{T}(x))$ are real and negative for all $x > x_*$, whereas for $x < x_*$ the eigenvalues can be non-real, but always have negative real parts.

Next, we characterize the discrete spectrum of L, *i.e.*, its isolated eigenvalues of finite multiplicity. An element $\lambda \in \sigma_{\text{disc}}(L)$ is such that there exists $(\tilde{\sigma}, \tilde{Z}) \neq (0, 0)$ satisfying

$$\lambda \begin{pmatrix} \tilde{\sigma} \\ \tilde{Z} \end{pmatrix} = J(\overline{\sigma}, \overline{Z}, \overline{T}) \begin{pmatrix} \tilde{\sigma} \\ \tilde{Z} \end{pmatrix} + \begin{pmatrix} (\overline{Z}+1)/\varepsilon \\ -\overline{\sigma}/\varepsilon \end{pmatrix} P\tilde{\sigma} \,. \tag{5.4}$$

Row manipulations and use of the steady state relationships $\overline{\sigma} = (\overline{Z}+1)(\overline{T}-\overline{\sigma})/\varepsilon$ and $\overline{Z} = -\overline{\sigma}(\overline{T}-\overline{\sigma})/\varepsilon$ show that this condition is equivalent to

$$\begin{pmatrix} \lambda + 1 + (\overline{Z}+1)/\varepsilon & \overline{Z}/\overline{\sigma} \\ (\lambda+2)\overline{\sigma} & (\lambda+2)\overline{Z} + \lambda + 1 \end{pmatrix} \begin{pmatrix} \tilde{\sigma} \\ \tilde{Z} \end{pmatrix} = \begin{pmatrix} (\overline{Z}+1)/\varepsilon \\ 0 \end{pmatrix} P\tilde{\sigma} \,. \tag{5.5}$$

Since $\lambda \notin \sigma_{\rm ess}(L)$, one can solve Eq. (5.5) for $(\tilde\sigma, \tilde Z)$ in terms of $P\tilde\sigma$. The solution is

$$\begin{pmatrix} \tilde\sigma \\ \tilde Z \end{pmatrix} = \begin{pmatrix} \Sigma(\lambda,x) \\ \mathcal{Z}(\lambda,x) \end{pmatrix} P\tilde\sigma \ , \tag{5.6}$$

where

$$\begin{aligned} \Sigma(\lambda,x) &:= \frac{[(\lambda+2)\overline{Z}+\lambda+1](\overline{Z}+1)/\varepsilon}{[(\lambda+2)\overline{Z}+\lambda+1][\lambda+1+(\overline{Z}+1)/\varepsilon]-(\lambda+2)\overline{Z}} \ , \\ \mathcal{Z}(\lambda,x) &:= \frac{-(\lambda+2)\overline{\sigma}(\overline{Z}+1)/\varepsilon}{[(\lambda+2)\overline{Z}+\lambda+1][\lambda+1+(\overline{Z}+1)/\varepsilon]-(\lambda+2)\overline{Z}} \ . \end{aligned} \tag{5.7}$$

We emphasize that the denominator in these expressions vanishes for some $x \in [-\frac{1}{2}, 0]$ if and only if $\lambda \in \sigma_{\rm ess}(L)$. The preceding calculations lead to the following characterization of the discrete spectrum:

Lemma 5.2: *A complex number λ belongs to $\sigma_{\rm disc}(L)$ if and only if $\lambda \notin \sigma_{\rm ess}(L)$ and*

$$24\int_{-1/2}^{0} x^2\Sigma(\lambda,x)\,dx = 1 \ . \tag{5.8}$$

Moreover, if $\lambda \in \sigma_{\rm disc}(L)$, then λ has multiplicity 1.

The integral in the eigenvalue condition (5.8) can be evaluated by changing variables from x to $s := \overline{v}_x(x)$ using the relation $-\overline{f}x = w(s)$ (*cf.* Eq. (3.6)):

$$1 - 24\int_{-1/2}^{0} x^2\Sigma(\lambda,x)\,dx = \frac{24}{\overline{f}^3}\int_{\mathcal{U}} w(s)^2\left[1-\tilde\Sigma(\lambda,s)\right]w'(s)\,ds \ , \tag{5.9}$$

where the interval of integration is $\mathcal{U} := [0, s_*^+] \cup [s_*^-, s_w]$ and

$$\tilde\Sigma(\lambda,s) := \frac{\lambda+1-s^2}{(\lambda+1)\left[1+\varepsilon(\lambda+1)\right]-\left[1-\varepsilon-\varepsilon(\lambda+1)^2\right]s^2+\varepsilon s^4} \ . \tag{5.10}$$

We define $\Phi(\lambda, \overline{T}_*, \delta)$ to be $\varepsilon\overline{f}^3/24$ times the right-hand side of Eq. (5.9), *i.e.*,

$$\Phi(\lambda,\overline{T}_*,\delta) := \int_{\mathcal{U}} \frac{s^2\left[(\lambda+1)^2+s^2\right]\left[1+\varepsilon+\varepsilon s^2\right]^2\left[1+\varepsilon-(1-2\varepsilon)s^2+\varepsilon s^4\right]}{(1+s^2)^3\left\{(\lambda+1)\left[1+\varepsilon(\lambda+1)\right]-\left[1-\varepsilon-\varepsilon(\lambda+1)^2\right]s^2+\varepsilon s^4\right\}}\,ds \ . \tag{5.11}$$

The functions Φ depends on the parameters $\overline{T}_*$ and δ through s_*^-, s_*^+, and s_w, which determine $\mathcal{U}$. As an immediate consequence of Lemma 5.2, we have the following characterization of the discrete spectrum of L.

Proposition 5.3: *The discrete spectrum of L is*

$$\sigma_{\rm disc}(L) = \left\{ \lambda \in C\backslash\sigma_{\rm ess}(L) \,|\, \Phi(\lambda,\overline{T}_*,\delta) = 0 \right\} \ . \tag{5.12}$$

While the integral in the definition of Φ can be evaluated explicitly, its exact form is not illuminating for computing the discrete spectrum analytically, and we determine it numerically as follows. A numerical scheme is used to solve the equation $\Phi(\lambda, \overline{T}_*, \delta) = 0$ for

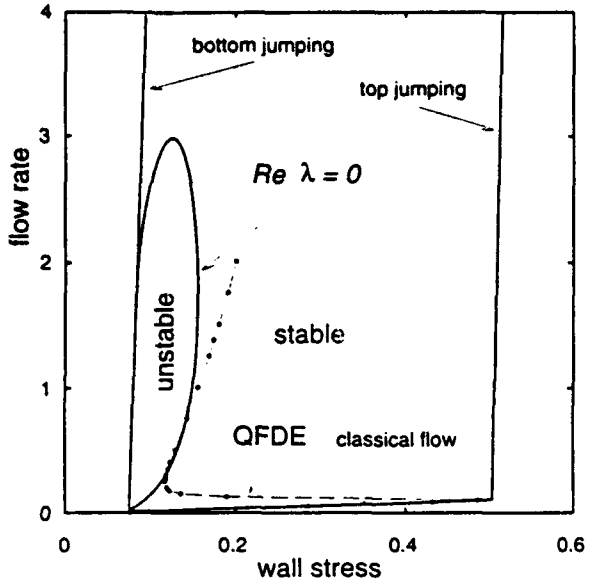

Fig. 4a: The regions of linearized stability and instability for steady state solutions with a single jump. The dots connected by dashed lines represent data from start-up simulations of system $(QFDE)$.

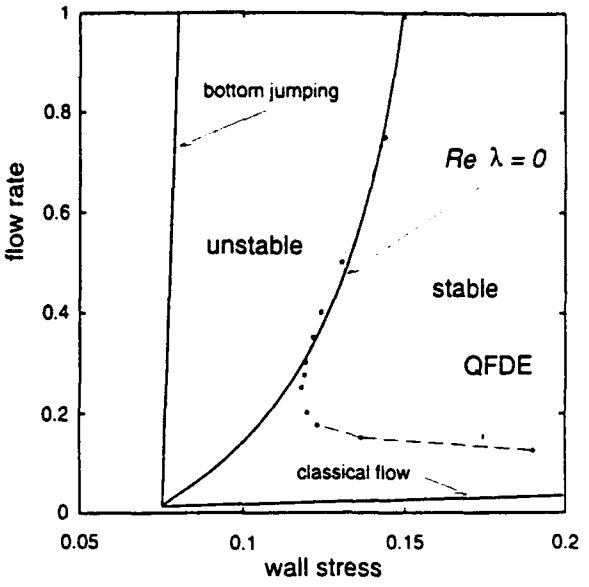

Fig. 4b: A closeup view of the portion of Fig. 6a where start-up simulations of system $(QFDE)$ leads to instability.

λ, given $\overline{T}_*$ and δ. This is a system of two real equations, $\mathrm{Re}\,\Phi(a+bi, \overline{T}_*, \delta) = 0$ and $\mathrm{Im}\,\Phi(a+bi, \overline{T}_*, \delta) = 0$, for the real and imaginary parts of $\lambda := a+bi$. We accounted for the possibility of having multiple roots by plotting the two level curves $\mathrm{Re}\,\Phi = 0$ and $\mathrm{Im}\,\Phi = 0$ in the (a,b)-plane using a contour plotter and looking for their intersections. For the range of parameters $\overline{T}_*$ and δ we explored, there is always exactly one intersection, and hence a single root.

We are interested in the possibility that this element λ of the discrete spectrum have $\mathrm{Re}\,\lambda > 0$, so that the corresponding steady state solution $(\overline{\sigma}, \overline{Z})$ is linearly unstable. Regarding λ now as a function of $\overline{T}_*$ and δ, instability would occur in a certain region of the $(\overline{T}_*, \delta)$-plane. The region in of instability is separated from the region of stability by the set of $(\overline{T}_*, \delta)$ such that $\mathrm{Re}\,\lambda = 0$. Thus we are led to find the curve of parameters $(\overline{T}_*, \delta)$ for which there exists a $b \in \mathbf{R}$ such that $\Phi(bi, \overline{T}_*, \delta) = 0$.

The results of solving this system of equations numerically is depicted in Fig. 4a. (The viscosity ratio is taken to be $\varepsilon = 0.001417$, which corresponds [3] to the polyisoprene sample PI-7 of Ref. [14].) Instead of plotting the $\mathrm{Re}\,\lambda = 0$ curve in the $(\overline{T}_*, \delta)$-plane, however, we have used as coordinates the wall stress $\overline{T}_w := \overline{T}_*/(1-2\delta)$ and the flow rate $\overline{Q}$, as given in Eq. (3.6).

6. Relation of Analysis to Simulation.

To compare the results from numerical simulation of $(QFDE)$ in Sec. 4 with the linearized stability analysis of Sec. 5, we observe that for each $\overline{Q} > 0$, the numerical solution of a start-up problem for $(QFDE)$ contains one parameter, δ, that approaches a constant value as

time tends to infinity. Associated with this value of δ and of $\overline{Q}$, there is a unique steady state $(\overline{\sigma}(x), \overline{Z}(x))$ (with a single jump discontinuity) having layer thickness δ and flow rate $\overline{Q}$: this steady state might not be stable, in which case the solution does not approach this steady state, but rather seems to tend to a limit cycle (in the σ, Z phase plane) that in some sense "encircles" the unstable steady state. This steady state, be it linearly stable or unstable, can be computed by solving the equation

$$\overline{Q} = Q_{steady}(\overline{T}_*, \delta) \tag{6.1}$$

for $\overline{T}_*$, where $Q_{steady}(\overline{T}_*, \delta)$ is the function defined by the right side of Yao's formula for the flow rate, Eq. (3.6), in which the relevant parameters have been written in terms of $\overline{T}_*$ and δ, using relations of Sec. 3.

We have simulated a sequence of start-up problems, with increasing values of $\overline{Q}$, and computed $\overline{T}_*$ for each value of δ obtained. This gives a sequence of points in the $(\overline{T}_*, \delta)$-plane. The results for $\varepsilon = 0.001417$ are plotted as the discrete points in Figs. 4a and 4b: the equivalent coordinates $(\overline{T}_w, \overline{Q})$ have been used, as described at the end of Sec. 5. Figure 4b shows that the curve defined by this set of points crosses transversely into and out of the unstable region as $\overline{Q}$ increases. The two crossing points correspond to the transition points between the oscillatory regime and the spurt I and II regimes, respectively. Thus the numerical results suggest that the region of linearly unstable steady states is explored by the dynamical start-up experiments. We emphasize that although some steady state solutions of $(QFDE)$ are linearly unstable, all solutions of $(QFDE)$ are bounded for all time (see, Sec. 2).

A plausible explanation of the observed behavior, as well as of the correspondence between the solutions of $(QFDE)$ and the linearized stability analysis, is that for increasing values of the flow rate $\overline{Q}$, $(QFDE)$ is undergoing Hopf bifurcation upon crossing into and out of a regime of periodic orbits. We prove such a result in Ref. [10] by showing how the infinite-dimensional flow problem generated by system $(QFDE)$ on the Hilbert space X is reduced (using the center manifold theorem) to one for a two-dimensional vector field to which the classical Hopf bifurcation theorem can be applied (see [11], Theorem 1.13). However, confirming that these periodic orbits are stable (hence observable in a physical experiment), requires showing that the bifurcation to periodic orbits is supercritical, and this remains an open problem for the present.

It is interesting to note that the frequency of these periodic orbits seems to have physical significance: in Ref. [9], the frequency is observed to be proportional to $1/\varepsilon$; according to the dimensional analysis leading to system $(QFDE)$ and the assumptions made in fitting model parameters to material data [3], this observation translates into a prediction that the dimensional frequency of oscillation is independent of molecular weight in a sequence of experiments varying molecular weight at the same fixed $\overline{Q}$. This seems to be the case with Lim's experimental data [4] to a reasonable degree of accuracy.

7. Conclusion

We have presented a mathematical model aimed at explaining the experiments of Lim and Schowalter. Our model of piston-driven channel shear flow of a highly elastic and very

viscous non-Newtonian fluid uses a constitutive model characterized by a non-monotonic relationship between steady shear stress and strain rate. We have described the reduction of the three-dimensional equations of motion and stress to approximating, one-dimensional systems that can be studied by a combination of numerical and analytic methods. The inertialess approximation results in a quadratic system of functional differential equations in which the prescribed volumetric flow rate is imposed by a feedback control. Numerical solution of this system exhibits four distinct flow regimes, as do the experiments of Lim and Schowalter. The third of these regimes exhibits persistent oscillations that compare favorably to the Lim-Schowalter observations.

If the governing system (JSO) and its inertial approximation ($QFDE$) model the observations of Lim and Schowalter correctly, then the details of the flow are different from what these experimentalists assumed. Rather than a stick-slip flow, the flow that we predict in the oscillatory regime has a thin "apparent slip" layer that exists for all time. The layer is unstable, in the sense that there are large and persistent time variations in the apparent slip velocity; these are associated with persistent oscillations in the pressure gradient that is controlled by fixing the flow rate $\overline{Q}$. For a certain range of $\overline{Q}$, we have provided convincing evidence that these oscillations are a consequence of a Hopf bifurcation to periodic orbits by a combination of analytical and computational methods. Moreover, the frequency of these oscillations agrees with observations of Lim. Our earlier analysis of the "spurt phenomenon" in Refs. [7, 12] explains why the control is the source of the instability: the flow would become steady if the control were removed by prescribing the pressure gradient (although, of course, the desired flow rate would then almost surely not be achieved).

REFERENCES

[1] M. Denn, "Issues in viscoelastic fluid dynamics," *Ann. Rev. Fluid Mech.* **22** (1989), 13–34.

[2] M. Johnson and D. Segalman, "A Model for Viscoelastic Fluid Behavior which Allows Non-Affine Deformation," *J. Non-Newtonian Fluid Mech.* **2** (1977), 255–270.

[3] R. W. Kolkka, D. S. Malkus, M. G. Hansen, G. R. Ierley, and R. A. Worthing, "Spurt Phenomena of the Johnson-Segalman Fluid and Related Models," *J. Non-Newtonian Fluid Mech.* **29** (1989), 303–325.

[4] F. J. Lim, "Wall slip in narrow molecular weight distribution polybutadienes," Ph.D. Thesis, Princeton Univ., 1988.

[5] F. J. Lim and W. R. Schowalter, "Wall Slip of Narrow Molecular Weight Distribution Polybutadienes," *J. Rheology* **33** (1989), 1359.

[6] D. S. Malkus, J. A. Nohel, and B. J. Plohr, "Dynamics of Shear Flow of a Non-Newtonian Fluid," *J. Comp. Phys.* **87** (1990), 464–487.

[7] D. S. Malkus, J. A. Nohel, and B. J. Plohr, "Analysis of New Phenomena in Shear Flow of Non-Newtonian Fluids," *SIAM J. Appl. Math.* **51** (1991), 899–929.

[8] D. S. Malkus, Y.-C. Tsai, and R. W. Kolkka, "New transient algorithms for non-Newtonian flows," *Finite Elements in Fluids* 8 (1992), 401–424.

[9] D. S. Malkus, J. A. Nohel and B. J. Plohr, "Approximation of piston-driven flows of a non-Newtonian fluid," in *Control Theory, Dynamical Systems, and Geometry of Dynamics*, (1993), Elworthy, Everitt, and Lee, Eds., Marcel Dekker, 173-192.

[10] D. S. Malkus, J. A. Nohel and B. J. Plohr, "Piston-driven shear flow of a non-Newtonian fluid," in preparation.

[11] J. E. Marsden and M. McCracken, *The Hopf Bifurcation and Its Applications*, Applied Mathematical Sciences 19, Springer-Verlag, New York, 1976.

[12] J. Nohel and R. Pego, "Nonlinear Stability and Asymptotic Behavior of Shearing Motions of a Non-Newtonian Fluid," *SIAM J. Math. Anal.* 24 (1993), 911–942.

[13] J. Oldroyd, "Non-Newtonian Effects in Steady Motion of Some Idealized Elastico-Viscous Liquids," *Proc. Royal Soc. London, Series A* 245 (1958), 278–297.

[14] G. V. Vinogradov, A. Ya. Malkin, Yu. G. Yanovskii, E. K. Borisenkova, B. V. Yarlykov, and G. V. Berezhnaya, "Viscoelastic Properties and Flow of Narrow Distribution Polybutadienes and Polyisoprenes," *J. Polymer Sci., Part A-2* 10 (1972), 1061–1084.

[15] M. Yao, "A Numerical and Analytical Study of Normal Stresses and Pressure Differences in non-Newtonian Creeping Flows," Ph.D. Thesis, Univ. of Wisconsin–Madison, 1989.

Department of Engineering Mechanics and the Center for the Mathematical Sciences, University of Wisconsin, Madison, WI 53706

E-mail: malkus@cms.wisc.edu

Forschungsinstitut für Mathematik, ETH-Zentrum, CH 8092 Zürich, Switzerland, and Department of Mathematics and the Center for the Mathematical Sciences, University of Wisconsin, Madison, WI 53706

E-mail: jan@math.ethz.ch

Departments of Mathematics and of Applied Mathematics and Statistics, State University of New York at Stony Brook, Stony Brook, NY 11794-3651

E-mail: plohr@ams.sunysb.edu